ELSEVIER

Journal of Fluids and Structures 22 (2006) 1097–1112

JOURNAL OF FLUIDS AND STRUCTURES

www.elsevier.com/locate/jfs

Flow structure of wake behind a rotationally oscillating circular cylinder

Sang-Joon Lee*, Jung-Yeop Lee

Department of Mechanical Engineering, Pohang University of Science and Technology, Pohang, 790-784, Republic of Korea

Received 17 September 2005; accepted 15 July 2006

Abstract

Flow around a circular cylinder oscillating rotationally with a relatively high forcing frequency has been investigated experimentally. The dominant parameters affecting this experiment are the Reynolds number (Re), oscillation amplitude (θ_A), and frequency ratio $F_R = f_f/f_n$, where f_f is the forcing frequency and f_n is the natural frequency of vortex shedding. Experiments were carried out under conditions of $\mathrm{Re} = 4.14 \times 10^3$, $0^\circ \leqslant \theta_A \leqslant 60^\circ$ and $0.0 \leqslant F_R \leqslant 2.0$. Rotational oscillation of the cylinder significantly modified the flow structure in the near-wake. Depending on the frequency ratio F_R, the cylinder wake showed five different flow regimes, each with a distinct wake structure. The vortex formation length and the vortex shedding frequency were greatly changed before and after the lock-on regime where vortices shed at the same frequency as the forcing frequency. The lock-on phenomenon always occurred at $F_R = 1.0$ and the frequency range of the lock-on regime expanded with increasing oscillation amplitude θ_A. In addition, the drag coefficient was reduced when the frequency ratio F_R was less than 1.0 ($F_R < 1.0$) while fixing the oscillation amplitude at $\theta_A = 30^\circ$. When the oscillation amplitude θ_A was used as a control parameter at a fixed frequency ratio $F_R = 1.0$ (lock-on regime), the drag reduction effect was observed at all oscillation amplitudes except for the case of $\theta_A = 30^\circ$. This type of active flow control method can be used effectively in aerodynamic applications while optimizing the forcing parameters.

Keywords: Rotational oscillation; Forcing frequency; Cylinder wake; Lock-on regime; Drag reduction; Flow control

1. Introduction

Fluid flow around a circular cylinder has been a major research topic for over a century due to its simple geometry and regular vortex shedding phenomenon. Reviews on the vortex shedding can be found in Bloor (1963), Gerrard (1966), Williamson (1996) and David and Gharib (2004). Many researchers have investigated the periodic shedding of vortices in flows around bodies and its effects on the bodies themselves. Interest in the formation and periodic shedding of large-scale vortices derives in part from the fact that these phenomena are responsible for structural vibrations and aero-acoustic noise, which can be detrimental factors in practical applications. Previous studies have established that the vortex shedding flow pattern varies according to the Reynolds number, making it possible to classify the flow around a circular cylinder into several flow regimes. Moreover, vortex shedding causes the drag and lift coefficients to

*Corresponding author. Tel.: +82 54 279 2169; fax: +82 54 279 3199.
E-mail addresses: sjlee@postech.ac.kr (S.-J. Lee), federex@postech.ac.kr (J.-Y. Lee).

0889-9746/$ - see front matter © 2006 Published by Elsevier Ltd.
doi:10.1016/j.jfluidstructs.2006.07.008

fluctuate and enhances turbulent mixing in the wake region. Therefore, many passive and active flow control techniques have been investigated to control the vortex structure in flows around a circular cylinder.

One type of active flow control method is the rotational oscillation technique. In this technique, an oscillating rotational motion is applied to the circular cylinder around which the fluid is flowing. The resulting mutual interaction between the rotationally oscillating body and adjacent fluid modifies the wake flow pattern by accelerating and decelerating the flow around the upper and lower parts of the cylinder. Depending on the forcing conditions, the flow behind a cylinder can be divided into three regimes, known as the non-lock-on, transition and lock-on regimes, each with a markedly different flow structure in the near-wake region behind the rotationally oscillating cylinder. Using the rotational oscillation technique, the flow structure can be modified so as to reduce the drag forces acting on the cylinder. In addition, in the lock-on flow regime, the vortex shedding frequency equals the frequency of the forced oscillation. The frequency range of the lock-on regime expands with increasing oscillation amplitude, and has been shown to encompass the natural vortex shedding frequency (Mahfouz and Badr, 2000; Ongoren and Rockwell, 1988).

Although the rotational oscillation technique is a promising and effective method for controlling the flow around bluff bodies, only a limited number of studies have examined this approach to active flow control. Taneda (1978) visualized the periodic shedding of vortices behind the rotationally oscillating cylinder for flows in the range of $30 \leqslant \mathrm{Re} \leqslant 300$ and $0 \leqslant \mathrm{St}_f\ (= f_f d/U_\infty) \leqslant 55$. He observed that applying high-frequency rotational oscillations to a cylinder caused the dead water region to vanish. Tokumaru and Dimotakis (1991) carried out similar experiments at a high Reynolds number of $\mathrm{Re} = 1.5 \times 10^4$. They reported that the wake behind a rotationally oscillating cylinder has four different flow modes depending on the forcing condition, and that the flow phenomenon may be qualitatively the same over a large range of Reynolds numbers. In addition, on the basis of indirect measurements, they found a drag reduction of about 80% at a very high forcing frequency. In a numerical investigation of the effect on the wake structure of rotational oscillatory motion, Mahfouz and Badr (2000) found that the wake structure strongly depended on the oscillation parameters. They found that the lock-on phenomenon occurred at forcing frequencies near the natural shedding frequency and that the frequency range over which this phenomenon occurred widened with increasing oscillation amplitude. Filler et al. (1991) measured the frequency response of the shear layers (and near-wake) in their experiment with Reynolds numbers ranging from 250 to 1200. They observed large velocity fluctuations and higher response peaks for frequencies near the Karman frequency of the test cylinder. This observation suggests that the response of the flow around the cylinder to the rotational oscillation of the cylinder is qualitatively similar to the response of an oscillator near resonance. Moreover, they observed a phase change of approximately 180° between the cylinder motion and the vortex shedding when the forcing frequency crossed the natural Karman frequency. In a study of the drag reduction mechanism and its effects, Shiels and Leonard (2001) showed that the reduction in drag was a result of separation delay due to the presence of a multipole vorticity structure in the boundary layer above the oscillating cylinder. They also found that the rotational oscillation technique is effective only at high Reynolds number ($\mathrm{Re} \geqslant 3000$).

Most previous studies on the rotational oscillation technique have been performed at relatively low Reynolds numbers with small forcing frequencies, and most researches have been based on numerical simulation. However, the ability to control flows at relatively large Reynolds numbers using high forcing frequencies is essential for practical applications. Moreover, the effectiveness of this active flow control technique needs to be checked by evaluating the amount of drag reduction and modification of the wake flow structure. In the present study, we therefore examined the modification of the flow structure of the wake behind a rotationally oscillating cylinder and drag reduction effect by varying the forcing conditions. To investigate the modification of flow structure under conditions similar to those encountered in practical applications, experiments were carried out under high forcing frequencies at a relatively high Reynolds number. The flow structure was measured using a hot-wire anemometry and visualized with smoke-wire flow visualization technique. The drag coefficient was evaluated indirectly from the wake velocity profiles. The variation of flow structure in the lock-on flow regime according to the oscillation amplitude θ_A and the forcing conditions that give large drag reduction are discussed in detail.

2. Experimental apparatus and method

2.1. Wind tunnel and experimental model

Experiments were performed in a closed-return type subsonic wind tunnel with a test section of 0.72 m (width) × 0.6 m (height) × 6.75 m (length). The free-stream turbulence intensity in the test section was less than 0.08% at $U_\infty = 10\,\mathrm{m/s}$. This level of turbulence intensity is sufficient to check the modification of wake structure

behind a bluff body (Gerrard, 1954). The cylinder model was a piece of acryl pipe of length $l = 400$ mm and diameter $d = 30$ mm. The free-stream velocity was $U_\infty = 2$ m/s and the corresponding Reynolds number based on the cylinder diameter was 4140. Since the aspect ratio of the cylinder model is $l/d = 13.3$, it can be roughly considered as a two-dimensional model (Graham, 1969). An end-plate was attached to each end of the cylinder model to maintain two-dimensional flow in the cylinder wake by minimizing the effect of the boundary layer developed along the wind tunnel sidewall. The shape and size of the end-plates were determined based on the results of Stansby (1974). A schematic diagram of the cylinder model and the coordinate system used in this study is shown in Fig. 1. The cylinder model was placed horizontally in the central region of the wind tunnel test-section. The blockage ratio of the tested cylinder and end-plates was about 8%. To account for the blockage ratio and wall interference effects, we used the formulas of Maskell (1963) to correct the velocity values.

In the experimental condition considered in the present work, the natural vortex shedding frequency (f_n) is 15.14 Hz. The Strouhal number based on the natural vortex shedding frequency and corrected free-stream velocity is $\mathrm{St}_n\ (= f_n d/U_\infty) = 0.214$. To achieve frequency ratios ($F_R = f_f/f_n$) of up to $F_R = 2.0$ (where f_f is the forcing frequency), a rotational oscillation device capable of generating oscillation frequencies higher than 30 Hz was designed. The device was connected to the test cylinder and driven by an AC servo motor. During the experiments, the oscillation amplitude was varied from $\theta_A = 0^\circ$ to 60°. The oscillatory motion of the cylinder and rotating motion of the driving motor can be represented as follows:

$$\theta_C = \tan^{-1}\left(\frac{\sin\,\theta_A\,\cos(\theta_m + \pi)}{\cos\,\theta_A}\right), \tag{1}$$

$$\theta_m(t) = 2\pi f_f t, \tag{2}$$

where θ_c, θ_m, θ_A and t indicate the phase angle of the cylinder oscillation ($-\theta_A \leqslant \theta_c \leqslant \theta_A$), and the phase angle of the motor rotation ($0 \leqslant \theta_m \leqslant 2\pi$), the angular amplitude of the rotational oscillation and time, respectively. Fig. 2 shows a schematic diagram of the rotational oscillatory motion of the circular cylinder.

2.2. Wake flow measurement and visualization

Fig. 3 shows the flow measurement system used in this study to measure the wake velocity. Wake velocity profiles were measured using an I-type hot-wire probe (DANTEC 55P11) connected to a constant temperature hot-wire anemometer (TSI IFA-100). The streamwise mean velocity and turbulence intensity profiles at $x/d = 4$ were measured

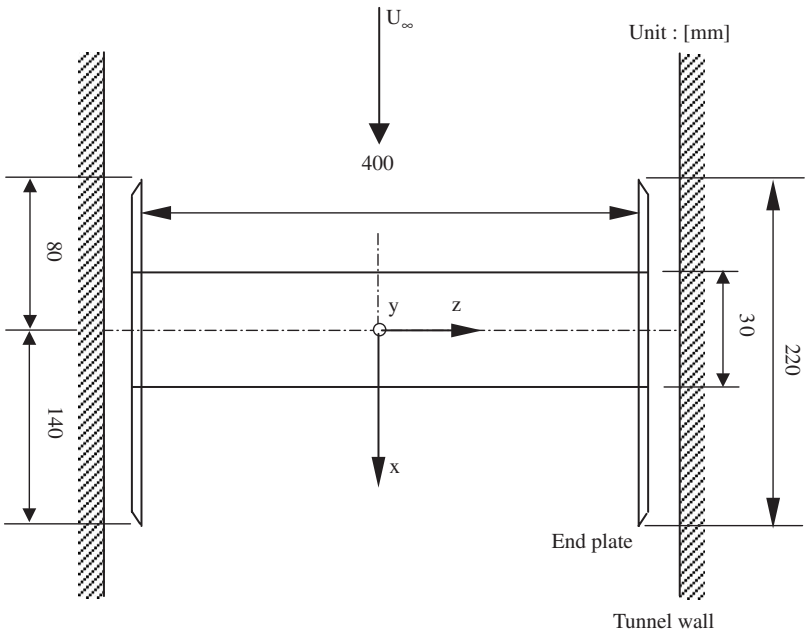

Fig. 1. Schematic diagram of test cylinder and coordinate system (units: mm).

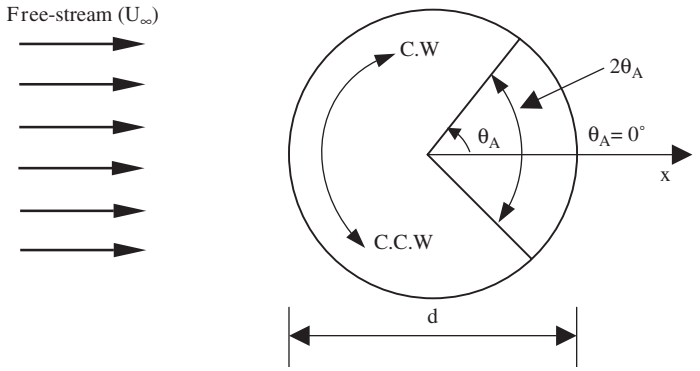

Fig. 2. Schematics of the rotationally oscillating motion of a circular cylinder.

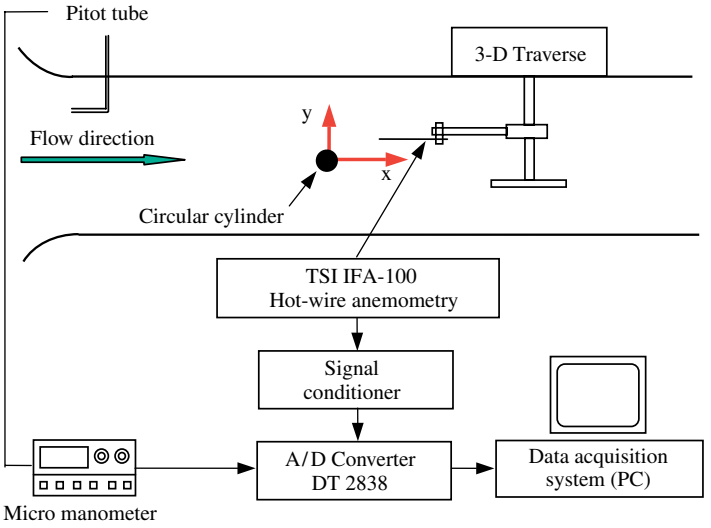

Fig. 3. Wind tunnel test-section and wake measurement system.

by traversing the hot-wire probe with an accuracy of 0.01 mm over the range $y/d = -3 \sim 3$ in intervals of $\Delta y = 0.1d$. At each measurement point, 16 384 velocity data were acquired at a sampling rate of 4000 samples/s with an A/D converter (DT2838), after low-pass filtering at 800 Hz. To investigate the vortex structure in the near wake, the velocity signals at the locations $x/d = 2$, $y/d = 0.5$ and $x/d = 10$, $y/d = 1$ were spectrally analyzed.

The drag coefficients (C_D) were evaluated indirectly by applying the following formulas suggested by Dimotakis (1978) to the streamwise mean velocity profile measured:

$$\frac{\delta^*}{h} = \int_0^1 \left[1 - \frac{u(\eta)}{U_o}\right] \mathrm{d}\eta, \tag{3}$$

$$D = \frac{2h/d}{(1-\delta^*/h)^2}\left[\int_0^1 \frac{u}{U_o}\left(1 - \frac{u}{U_o}\right)\mathrm{d}\eta - \frac{1}{2}\left(\frac{\delta^*}{h}\right)^2\right], \tag{4}$$

where h, η and U_o are the vertical length of measurement ($-3 \leqslant y/d \leqslant 3$), the normalized vertical position (y/h), and the velocity in the region outside the cylinder wake, respectively. The drag coefficients determined in this way were normalized with that of the stationary cylinder (C_{Do}).

The flow pattern around the test cylinder was visualized using the smoke-wire method. Briefly, a nichrome wire of diameter 0.1 mm was installed vertically at 90 mm upstream of the cylinder model. The wire was painted with SAFEX fog fluid and then the wire was heated by applying an electric pulse using a DC power supply. Small fog fluid droplets

were evaporated from the wire and then dense white smoke filaments were produced. The smoke was illuminated with a laser beam issuing from an Nd:Yag pulsed laser, which was passed through mirrors and a cylindrical lens to form a thin laser light sheet. To obtain clear flow images of the turbulent wake, the Nd:Yag pulsed laser was synchronized with the DC power supply. Instantaneous wake flow images were captured with a digital camera (Nikon D100).

3. Results and discussion

3.1. Spectral analysis

Fig. 4 shows the power spectral density (PSD) distributions measured at the downstream locations $x/d = 2$, $y/d = 0.5$ and $x/d = 10$, $y/d = 1$. In these distributions, a distinct peak indicates the existence of a dominant vortex structure due to periodic vortex shedding, and the peak frequency corresponds to the vortex shedding frequency. Depending on the vortex shedding frequency (f_s), the wake flow behind the rotationally oscillating cylinder can be classified into five different flow regimes, and the vortex shedding phenomena show quite different characteristics before and after the lock-on regime.

For $F_R \leqslant 0.6$ (Figs. 4(a) and (b)), vortex shedding occurs at the natural frequency (f_n). This range of F_R thus corresponds to the low-frequency non-lock-on regime where vortices shed at the natural frequency, irrespective of the forced oscillation frequency (f_f). This non-lock-on behavior occurs when the difference between the natural frequency and the forcing frequency is large. At $F_R = 0.8$ (Fig. 4(c)), the peak corresponding to the vortex shedding frequency is weaker, but still clear, and a dominant peak is observed at the forcing frequency. This flow regime is called the low-frequency transition regime.

At $F_R = 1.0$ and 1.2 (Figs. 4(d) and (e), respectively), the only feature in the PSD distribution is a single dominant peak at the forcing frequency. In this flow regime, known as the lock-on regime, vortices shed at the same frequency as the forcing frequency ($f_s = f_f$). The wake structure is synchronized with the oscillatory motion of the test cylinder and the interaction becomes active. Our results are consistent with previous findings showing that the lock-on phenomenon occurs over a frequency range that encompasses the natural frequency. Previous studies have also shown that the frequency range of the lock-on regime widens with increasing the oscillation amplitude. Fig. 5 shows the variation of the lock-on range with respect to the oscillation amplitude in our experiments. For comparison, Fig. 5 includes the qualitative frequency-selection diagram of Mahfouz and Badr (2000), who found that the lock-on range increases linearly with oscillation amplitude. The lock-on phenomenon always occurs at $F_R = 1.0$ and its range expands as the oscillation amplitude increases, consistent with the predictions of Baek and Sung (1998), Ongoren and Rockwell (1988) and Mahfouz and Badr (2000). However, as shown in Fig. 5, this expansion is not linear; rather, it shows a somewhat zigzag pattern centered at $F_R = 1.0$.

As the oscillation amplitude decreases, the lock-on range narrows until a certain threshold amplitude (θ_t) is reached. Below θ_t, the lock-on phenomenon occurs only at $F_R = 1.0$. Koopman (1967) reported the existence of a threshold value of this type in his experimental study of flow around a cylinder undergoing transverse oscillation. However, the exact threshold value has not yet been established. In this experiment, the threshold value was found to be $\theta_t = 8^\circ$, indicating that the lock-on phenomenon occurs in the range of $\theta_A \leqslant 8^\circ$ only at the frequency ratio of $F_R = 1.0$. The finding of this threshold value seems to be attributed to the precise control of oscillation amplitude and high forcing frequency tested in this experiment.

On further increase of the forcing frequency to $F_R = 1.6$, two distinct peaks, one at the vortex shedding frequency and the other at the forcing frequency, appear again. This is classified as the high-frequency transition regime. In this regime, the vortex shedding frequency is relatively low, possibly as a result of non-synchronization between the oscillatory motion of the cylinder and the wake flow after deviating from the lock-on regime. This flow characteristic will be discussed in detail below in relation to Fig. 6.

Still further increase of the forcing frequency to $F_R = 2.0$ (Fig. 4(g)) pushes the flow regime into the high-frequency non-lock-on regime. In this frequency ratio, the PSD distributions measured for the near-wake ($x/d = 2$) and far-wake ($x/d = 10$) regions differ significantly. This difference can be attributed to the vortex coalescence phenomenon that occurs just behind the cylinder. In the near-wake PSD distribution, three distinct peaks are observed. The first peak represents the vortex shedding frequency (f_s) which recovered from the high-frequency transition regime, and the second and third peaks correspond to the frequency due to vortex coalescence (f_{vc}) and the forcing frequency (f_f), respectively. The third peak has very small amplitude, compared with the other two peaks.

In the far-wake PSD distribution, however, a single peak appears near the natural shedding frequency (f_n) and it is difficult to discern a distinct peak at the forcing frequency. Based on these results, we can conjecture that the

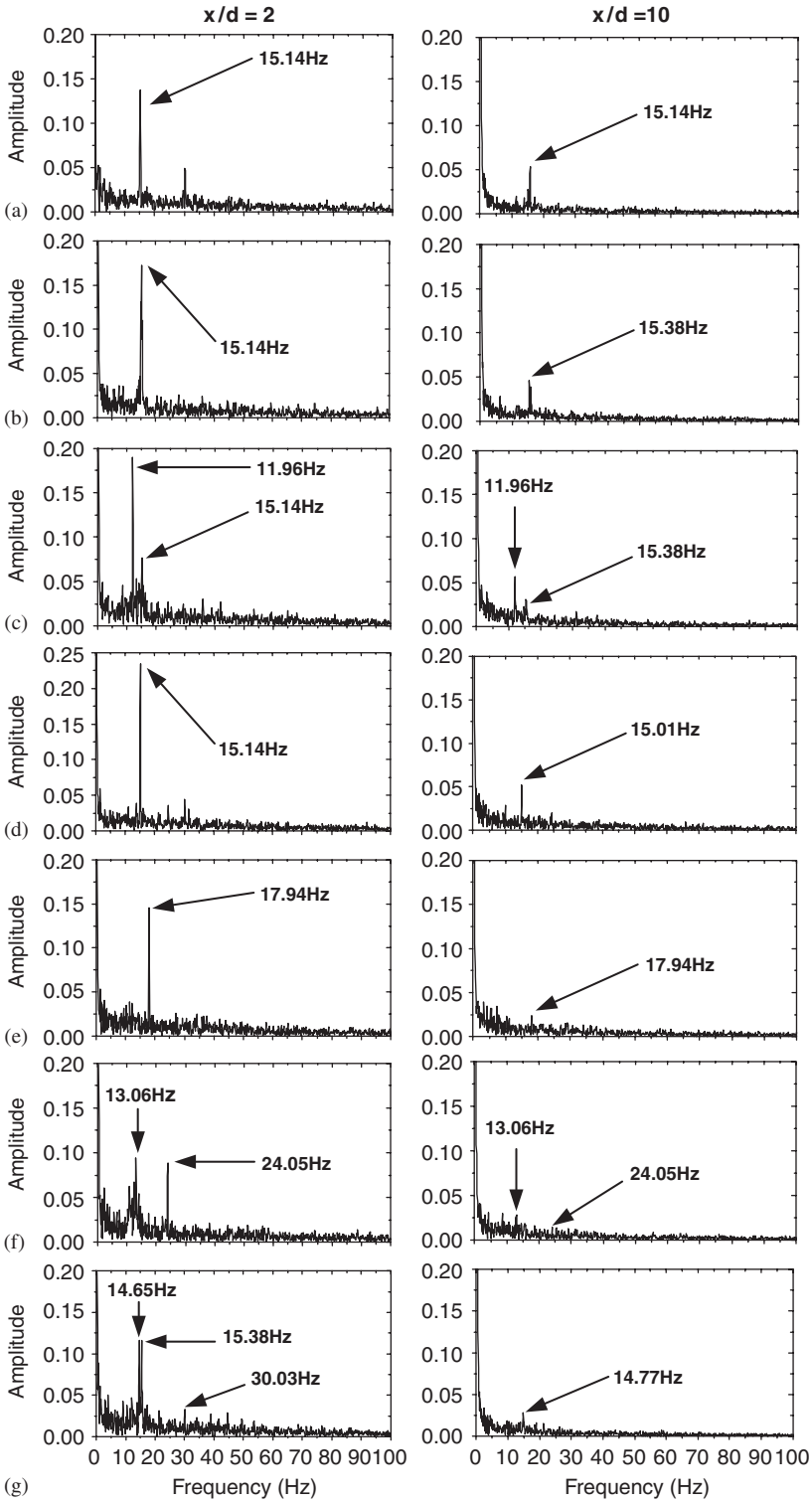

Fig. 4. Comparison of PSD distributions at $\theta_A = 30^\circ$. (a) $F_R = 0.0$, (b) $F_R = 0.4$, (c) $F_R = 0.8$, (d) $F_R = 1.0$, (e) $F_R = 1.2$, (f) $F_R = 1.6$, (g) $F_R = 2.0$; the natural vortex shedding frequency of a stationary cylinder ($F_R = 0.0$) is $f_n = 15.14$ Hz.

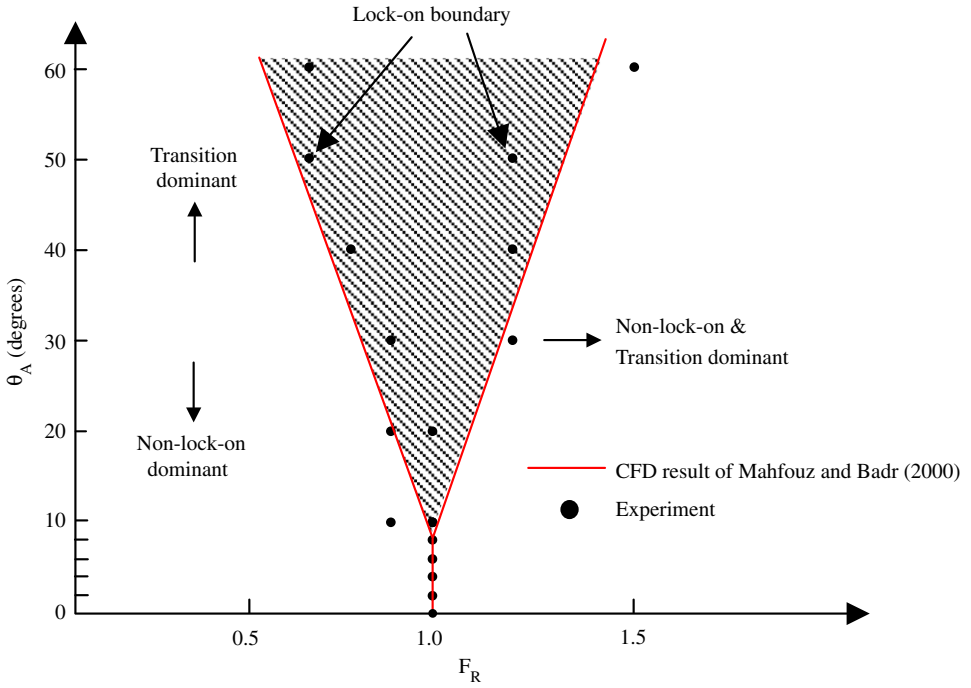

Fig. 5. Variation of lock-on range with respect to frequency ratio F_R and oscillation amplitude θ_A.

high-frequency rotational oscillation induces vortex coalescence in the near-wake region, and downstream of this vortex coalescence the vortices are shed with a single frequency. This agrees well with the numerical and experimental results of Choi et al. (2002) and Ongoren and Rockwell (1988). The present results thus confirm that the wake behind a rotationally oscillating cylinder can be classified into five flow regimes depending on the frequency ratio; this classification is summarized in Table 1.

Fig. 6 shows the variation of the vortex shedding frequency in the high-frequency transition regime. In this regime, the vortex shedding frequency is lower than the natural vortex shedding frequency of the stationary circular cylinder ($f_n = 15.14$ Hz). As F_R increases, the vortex shedding frequency increases and approaches near the natural frequency of vortex shedding. This seems to be due to the following two aspects. When the lock-on regime shifts to the high-frequency transition regime, the wake flow is strongly influenced by the high-frequency rotational oscillatory motion of the cylinder. In this flow regime, a large amount of angular momentum is transferred to the flow, which makes the flow follow the forcing motion. However, at high forcing frequencies there is no longer synchronization between the cylinder motion and flow adjacent to the cylinder surface. Eventually, the vortices shed at lower frequency than the natural vortex shedding frequency. Secondly, the motion of the cylinder and the vortex shedding of the flow are in phase in the lock-on regime. When the flow regime shifts to the high-frequency transition regime, the cylinder motion and vortex shedding become 180° (π) out of phase (Baek and Sung, 1998; Filler et al., 1991). This change in phase may also be responsible for the observed variation of the shedding frequency in the high-frequency transition regime. As a consequence of the non-synchronization between the two flow regimes, PSD peaks appear at frequencies lower than the natural frequency and the shedding frequency gradually recovers to the natural frequency as F_R is increased. These vortex shedding characteristics are quite different from those in the low-frequency transition regime, although both transition regimes have two distinct peaks.

3.2. Flow characteristics and drag coefficient

Fig. 7 shows the streamwise mean velocity and turbulence intensity profiles measured at the downstream location of $x/d = 4$ for $\mathrm{Re} = 4.14 \times 10^3$ and $\theta_A = 30^\circ$. In the non-lock-on regime with small frequency ratio F_R, the deficit of the streamwise velocity component gradually decreases with increasing F_R. The turbulence intensity distribution shows a typical double-peak shape. A decrease in the velocity deficit indicates that the momentum transfer from the outer wake

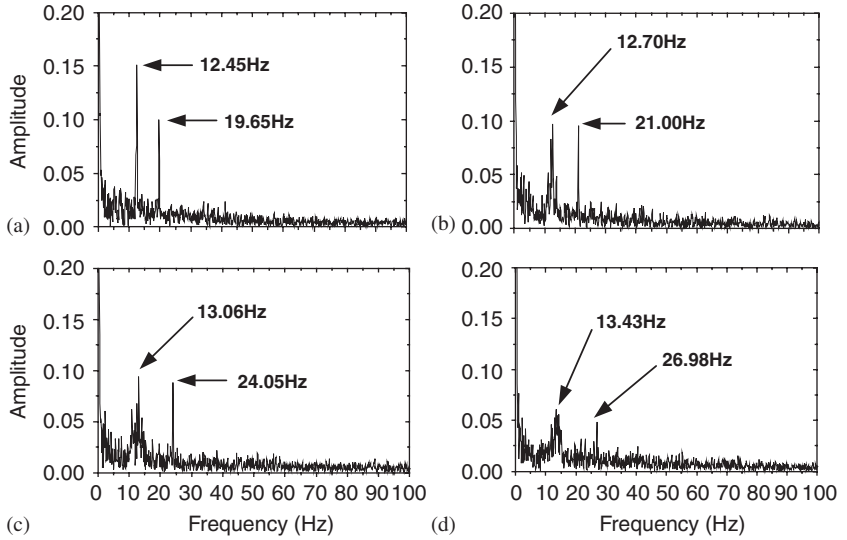

Fig. 6. Variation of vortex shedding frequency in the high-frequency transition regime at $x/d = 2$. (a) $F_R = 1.3$, (b) $F_R = 1.4$, (c) $F_R = 1.6$, (d) $F_R = 1.8$.

Table 1
Classification of flow regimes with respect to F_R

Frequency ratio (F_R)	Flow regime
$0 \leqslant F_R \leqslant 0.6$	Low-frequency non-lock-on regime
$0.6 < F_R < 0.9$	Low-frequency transition regime
$0.9 \leqslant F_R \leqslant 1.2$	Lock-on regime
$1.2 < F_R < 2.0$	High-frequency transition regime
$F_R \geqslant 2.0$	High-frequency non-lock-on regime

region compensates the velocity deficit in the wake center region due to the rotational oscillation motion of the cylinder. In particular, the largest decrease in the velocity deficit is observed at $F_R = 0.8$. In addition, the velocity profile has a nearly uniform distribution and the streamwise turbulence intensity is increased in the outer wake region.

On increasing F_R beyond the lock-on regime, the streamwise mean velocity takes on a bell-shaped distribution similar to that observed for the stationary cylinder ($F_R = 0.0$). However, the velocity deficit is increased and the turbulence intensity profiles become uniform in the wake center region. This behavior seems to be derived from the forcing-induced enhancement of flow separation. The high-frequency rotational oscillations change the vortex shedding characteristics and induce vortex coalescence by increasing the instability in the separated shear layer. In addition, the size of vortices generated in the upper and lower sides of the cylinder is smaller than that for the cases of $F_R < 1.0$. Moreover, these small vortices are located inside the relatively narrow wake region behind the cylinder without active motion for momentum exchange and convected to downstream. These flow features reduce momentum transfer from the outer wake region to the wake center region. This was confirmed by visualizing the flows around the test cylinder (see Section 3.3). The special features of the velocity deficit observed in Fig. 7 may result from the effects described above.

The streamwise mean velocity and turbulence intensity profiles were measured once again at the same downstream location to investigate the effect of the amplitude of the oscillatory motion (θ_A) applied to the test model at $F_R = 1.0$ in the lock-on regime. As shown in Fig. 8, the mean velocity profiles show nonlinear variation with respect to the oscillation amplitude. At $\theta_A = 10^\circ$, the velocity deficit is decreased by about 30% compared with the stationary cylinder. However, the velocity deficit increases as the oscillation amplitude is increased in the range of $\theta_A = 20^\circ - 40^\circ$. Further increase of the oscillation amplitude above $\theta_A = 40^\circ$ causes the velocity deficit to decrease, reaching a minimum value at $\theta_A = 60^\circ$. This non-linear behavior in the mean velocity profiles shown in Fig. 8 may be attributed to the different dynamic response of the flow to the oscillating cylinder, depending on the oscillation amplitude. These results

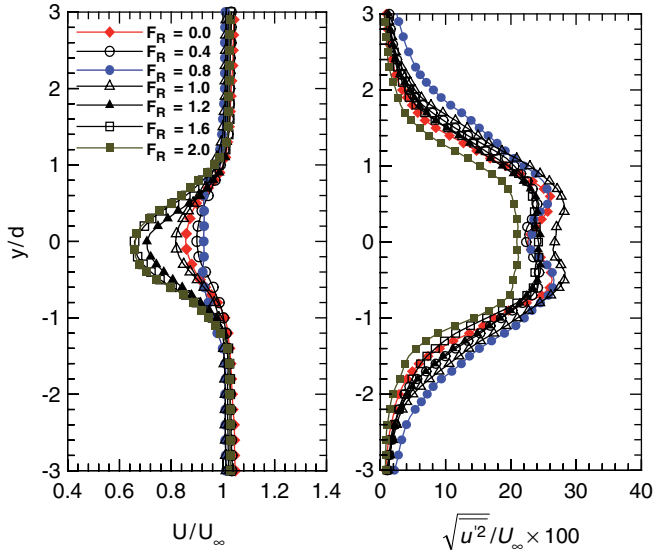

Fig. 7. Streamwise mean velocity and turbulence intensity profiles at $x/d = 4$ for $\mathrm{Re} = 4.14 \times 10^3$ and $\theta_A = 30^\circ$.

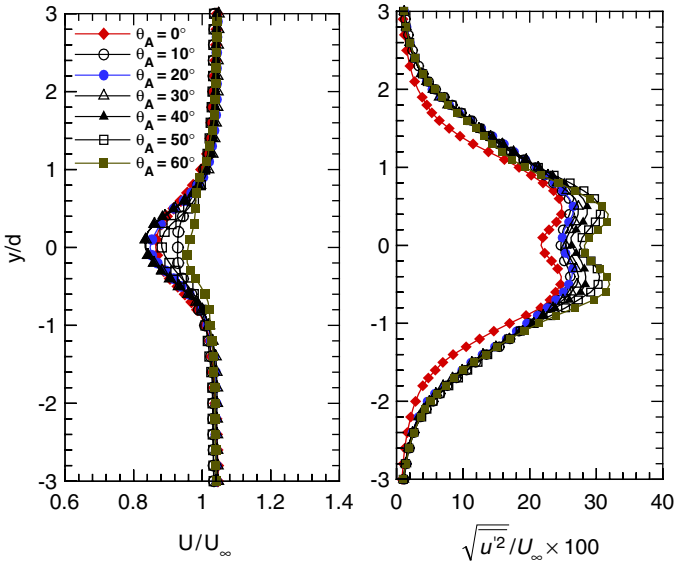

Fig. 8. Streamwise mean velocity and turbulence intensity profiles at $x/d = 4$ for $\mathrm{Re} = 4.14 \times 10^3$ and $F_R = 1.0$.

show that the wake structure strongly depends on the oscillation amplitude, even at the same forcing frequency ratio in the lock-on regime.

All of the turbulence intensity profiles in Fig. 8 exhibit distinct double peaks in the shear layers of the wake region. The local maxima increase in magnitude as the oscillation amplitude is increased. For all values of θ_A in the lock-on regime at $F_R = 1.0$, the turbulence intensity is greater than that observed for the stationary cylinder.

The variation of drag coefficient ratio (C_D/C_{Do}) as a function of the frequency ratio (F_R), determined using the momentum theorem based on the streamwise mean velocity distribution at $\theta_A = 30^\circ$, is shown in Fig. 9. The drag coefficient is reduced to below the value for the stationary cylinder only when $F_R < 1.0$. In the low-frequency transition regime, the maximum drag reduction is about 32.82% at $F_R = 0.8$. As F_R increases beyond the lock-on regime, however, the drag coefficient is increased greatly. At $F_R = 2.0$, for example, the drag is increased by about 80.9%. This

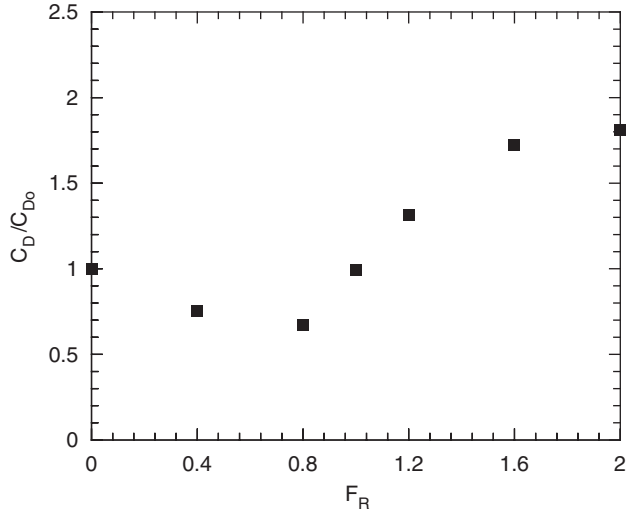

Fig. 9. Variation of drag coefficient ratio (C_D/C_{Do}) with respect to the frequency ratio F_R at $\theta_A = 30^\circ$.

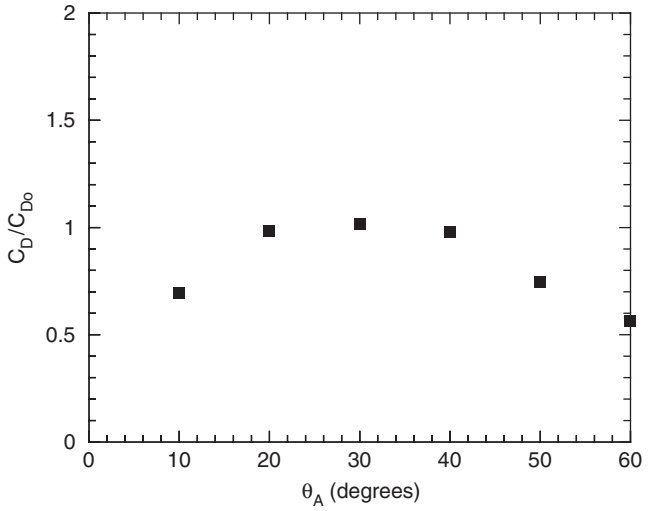

Fig. 10. Variation of drag coefficient ratio (C_D/C_{Do}) with respect to the oscillation amplitude θ_A at $F_R = 1.0$.

increase in drag at higher forcing frequencies is attributed to insufficient momentum transfer from the outer wake region to the wake center due to suppression of flow entrainmnet.

Fig. 10 shows the variation of the drag coefficient ratio (C_D/C_{Do}) as a function of the oscillation amplitude θ_A at $F_R = 1.0$. The drag coefficient is less than that of the stationary cylinder at all oscillation amplitudes, except only when $\theta_A = 30^\circ$. The drag reduction is large at low and high amplitudes, with values of 30.42% and 25.47% at $\theta_A = 10^\circ$ and 50°, respectively. However, it is only about 2% for the intermediate amplitudes of $\theta_A = 20^\circ$ and 40°. The largest drag reduction (43.7%) was observed at $\theta_A = 60^\circ$. This selective drag reduction effect centered at $\theta_A = 30^\circ$ may be due to different dynamic response of the flow to the oscillating cylinder, depending on the oscillation amplitude as explained in Fig. 8. From these results, we can see that the optimum forcing condition for drag reduction is $F_R < 1.0$ when the frequency ratio is used as a control parameter at a fixed oscillation amplitude θ_A. Especially, the drag reduction effect is large in the low-frequency transition regime. In addition, when the oscillation amplitude θ_A is used as a control parameter while fixing the frequency ratio at $F_R = 1.0$, the optimum condition for drag reduction is to deviate the oscillation amplitude from $\theta_A = 30^\circ$ as large as possible.

In order to measure the dynamic response of the near wake in the lock-on flow regime, the fluctuating velocity components at the forcing frequency were extracted after signal processing the hot-wire signals. Fig. 11 shows the variation of the fluctuating streamwise velocity component measured at a point in the near wake ($x/d = 2$, $y/d = 0.5$) with varying the oscillation amplitude θ_A under the condition of $\mathrm{Re} = 4.14 \times 10^3$ and $F_R = 1.0$. The near-wake response remains almost constant up to $\theta_A = 30^\circ$, and then increases linearly with increasing the oscillation amplitude. This near-wake response seems to be responsible for the selective drag reduction effect centered at $\theta_A = 30^\circ$. Fig. 11 agrees with the results of Filler et al. (1991) who detected the response by using the synchronous (lock-on amplifier) detection method at a low oscillation amplitude.

Bloor (1963) defined the end of the vortex formation region behind a circular cylinder as the location after which oscillating wake characteristics are observed. Gerrard (1966) also mentioned that the length of the vortex formation region could be obtained from the streamwise velocity fluctuations. Because the vortices shed from the two sides of the cylinder cross the wake center axis at the end of the formation region, the streamwise velocity fluctuations have a maximum root-mean-square (r.m.s.) value at the location. To investigate the length of the vortex formation region, we measured the streamwise turbulence intensity by traversing a hot-wire probe along the wake center-line. The vortex formation length was determined by detecting the peak location in a sixth-order polynomial fit of the turbulence intensity distribution. The vortex formation lengths obtained at various values of F_R are listed in Table 2. As can be seen in Fig. 12, when the frequency ratio is less than 1.0 ($F_R \leqslant 1.0$), the streamwise turbulence intensity increases initially and then reaches a peak value at a certain downstream location. However, the location of this peak shifts toward the cylinder as F_R is increased, indicating a decrease in the vortex formation length. At $F_R = 1.0$, the vortex formation region is the smallest, less than half that of the stationary cylinder ($F_R = 0.0$). The small length of the vortex formation region at low-frequency ratios reflects the strong influence of alternating shedding of large-scale vortices in the wake center region. The vortex shedding just behind the cylinder seems to be mainly attributed to increased vorticity in the shear layer due to the rotational oscillation of the cylinder. As mentioned by Shiels and Leonard (2001), the drag reduction effect seems to be due to separation delay resulting from a multipole vorticity structure. Their results match well with the drag reductions observed here for $F_R < 1.0$ and the strong influence of vortex shedding, as shown in Figs. 9 and 12. At $F_R = 1.2$, no distinct peak is observed in the turbulence intensity distribution because the turbulence

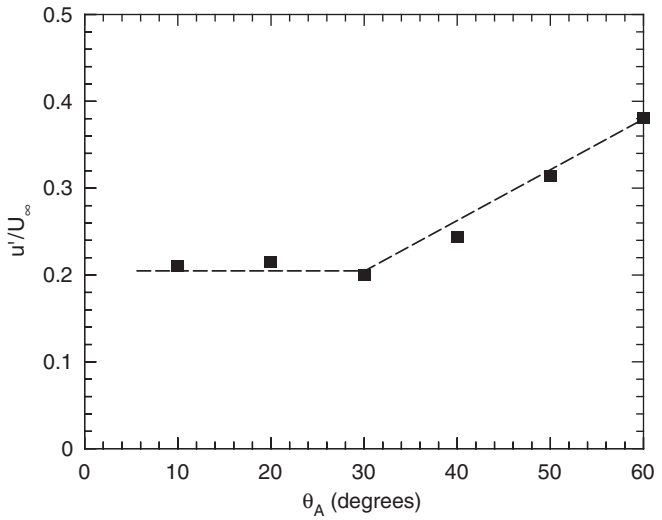

Fig. 11. Variation of streamwise velocity fluctuations u' at the forcing frequency measured at a point $x/d = 2$, $y/d = 0.5$ with varying the oscillation amplitude θ_A for $\mathrm{Re} = 4.14 \times 10^3$ and $F_R = 1.0$.

Table 2
Length of vortex formation region (x/d) with respect to F_R at $\theta_A = 30^\circ$

F_R	0.0 (Stationary)	0.4	0.8	1.0	1.2	1.6	2.0
x/d	2.85	2.06	1.31	1.08	—	—	—

intensity varies only to a small extent with moving downstream, possibly because vortex shedding occurs very close to the cylinder at this frequency ratio. At even higher frequency ratios, the promotion of separation causes a reduction in the influence of large-scale vortices on the wake center region.

In the lock-on flow regime, the effect of varying the oscillation amplitude has a similar effect on the flow as that observed when the frequency ratio was varied (Fig. 12). Fig. 13 shows the turbulence intensity distributions along the wake center-line at $F_R = 1.0$ under different oscillation amplitudes. The variation in the vortex formation length as a function of oscillation amplitude θ_A is summarized in Table 3. Although, for all non-zero values of θ_A, the vortex

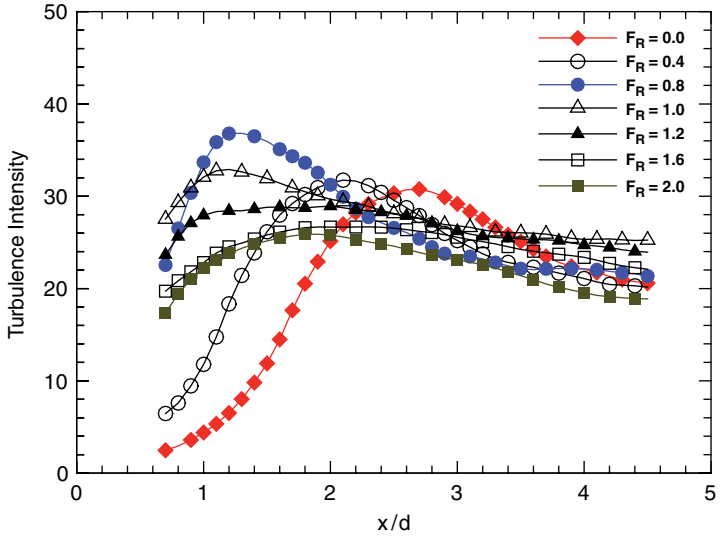

Fig. 12. Streamwise turbulence intensity distributions along the wake center-line for $\mathrm{Re} = 4.14 \times 10^3$ and $\theta_A = 30^\circ$.

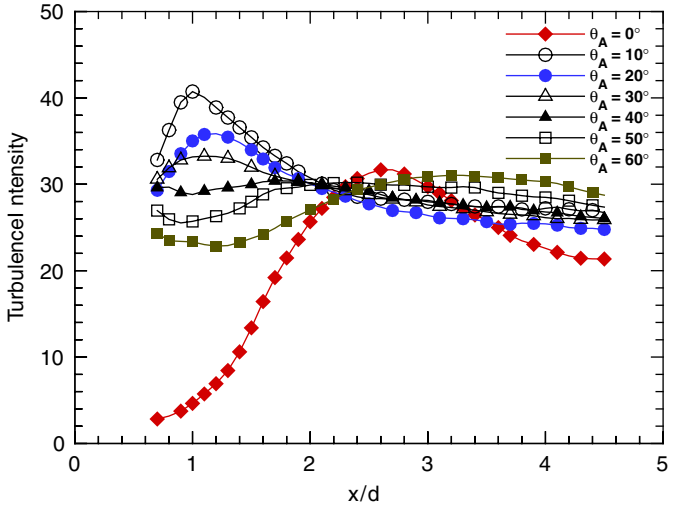

Fig. 13. Streamwise turbulence intensity distributions along the wake center-line for $\mathrm{Re} = 4.14 \times 10^3$ and $F_R = 1.0$.

Table 3
Length of vortex formation region (x/d) with respect to θ_A in the lock-on regime

θ_A	0° (Stationary)	10°	20°	30°	40°	50°	60°
x/d	2.85	1.05	1.15	1.08	—	—	—

formation length is less than that of the stationary cylinder, the peak location is relatively insensitive to θ_A. When $\theta_A \geqslant 40^\circ$, the turbulence intensity distributions do not show any clear peaks, because the vortices are shed just behind the cylinder. Based on these results, we can see that rotational oscillatory motion of a circular cylinder increases the velocity fluctuations in the near wake and shortens the length of vortex formation region.

The drag reduction in the lock-on flow regime seems to be caused by forcing the shear layer vortex shedding and delay (or suppression) of flow separation due to the synchronized wake structure at near the cylinder surface by the oscillatory motion of the cylinder as shown in Fig. 15. These effects are observed in a stationary cylinder wake at higher Reynolds number. It has been known that the drag coefficient decreases before the critical Reynolds number ($\mathrm{Re}_{cr} \approx 5.25 \times 10^5$) as the Reynolds number increases (Panton, 1996). This fact can support the drag reduction effect shown in the present study well. In addition, the momentum transfer from the outside of the wake region is enhanced due to the strong vortex motion. This also seems to attribute to reduce the drag force acting on the cylinder.

3.3. Flow visualization

Fig. 14 shows visualizations of the instantaneous flow structures in the vertical center plane of behind the test cylinder subjected to rotational oscillations of amplitude $\theta_A = 30^\circ$ at various values of the frequency ratio F_R. For F_R values up to 1.0 (Figs. 14(b)–(d)), the vortex formation length is much shorter than that of the stationary cylinder (Fig. 14(a)) and gradually decreases with increasing F_R. Therefore, vortex shedding occurs very near the cylinder due to increased vorticity in the shear layer induced by the oscillatory motion of cylinder. Moreover, the large-scale vortices shed from the oscillating cylinder are more regular and energetic, compared with those shed from the stationary cylinder. When the forcing frequency is high (Figs. 14(e) and (f)), it is difficult to discern a distinct and periodic vortex structure, and the vortices in the shear layer do not penetrate the wake center-line. Therefore, momentum transfer from inviscid flow into

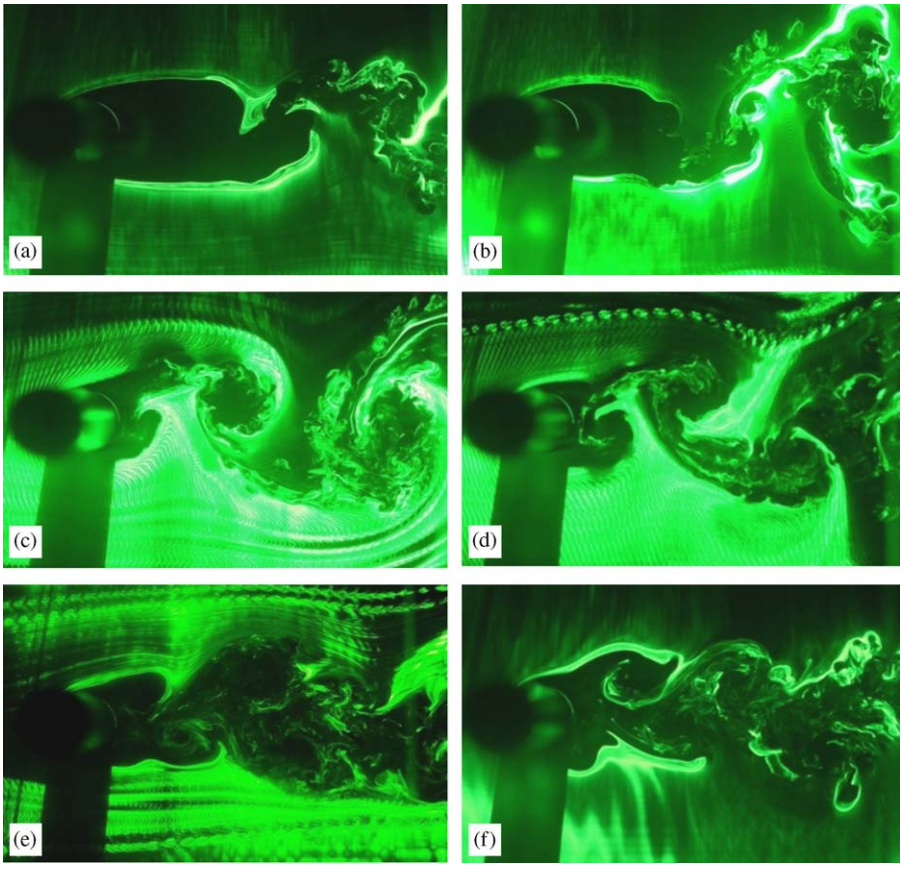

Fig. 14. Visualized flows in the vertical center plane according to the frequency ratio at $\theta_A = 30^\circ$. (a) Stationary, (b) $F_R = 0.4$, (c) $F_R = 0.8$, (d) $F_R = 1.0$, (e) $F_R = 1.6$, (f) $F_R = 2.0$.

the wake center region is suppressed and it is difficult to determine the vortex formation length. The promotion of flow separation and suppression of momentum transfer by the oscillatory motion are the principal factors for the gradual increase of drag coefficient under the conditions of $F_R > 1.0$. Moreover, the high-frequency rotational oscillatory motion of the cylinder increases coherence in the flow and then induces vortex coalescence. For this reason, only one frequency peak is observed in the far-wake at high-frequency ratios (see Fig. 4(g)).

Fig. 15 shows the effect of varying the oscillation amplitude θ_A on the visualized flow in the lock-on flow regime at $F_R = 1.0$. For all of the oscillation amplitudes studied, the vortex formation region is much shorter than for of the stationary cylinder. Moreover, the scale of the vortices decreases and fluctuations in the flow increase as the oscillation amplitude is increased. These observations are consistent with the increase in turbulence intensity with increasing θ_A described above (see Fig. 8). In addition, the vertical distance between the large-scale vortices shed from the upper and lower sides of the cylinder is also decreased. This results in high-speed active flow motion in the center region of the near wake just behind the cylinder, which effectively recovers the velocity deficit. Fig. 15(f) clearly shows the reason why the largest drag reduction was observed under the conditions of $F_R = 1.0$ and $\theta_A = 60^\circ$. Specifically, at the high oscillation amplitudes ($\theta_A = 50^\circ$ and 60°), a small-scale vortex is formed close to the cylinder surface, resulting in increased entrainment of smoke filaments. Fig. 16 shows the generation of this small-scale vortex in detail. This small-scale vortex formed in the shear layer at high oscillation amplitudes ($\theta_A = 50^\circ$ and 60°) may be related with the forced shear layer (or secondary) vortex shedding mentioned by Filler et al. (1991). In addition, in the lock-on flow regime, the large-scale vortex shedding is in phase with the oscillatory motion of the cylinder.

The qualitative visualizations of the flow structures provide good support for the quantitative results discussed earlier in this paper. Collectively, the present results indicate that the rotational oscillation of the cylinder controls the instability of the shear layer behind the cylinder, greatly influencing the wake structure, and can be used as an effective flow control method for drag reduction.

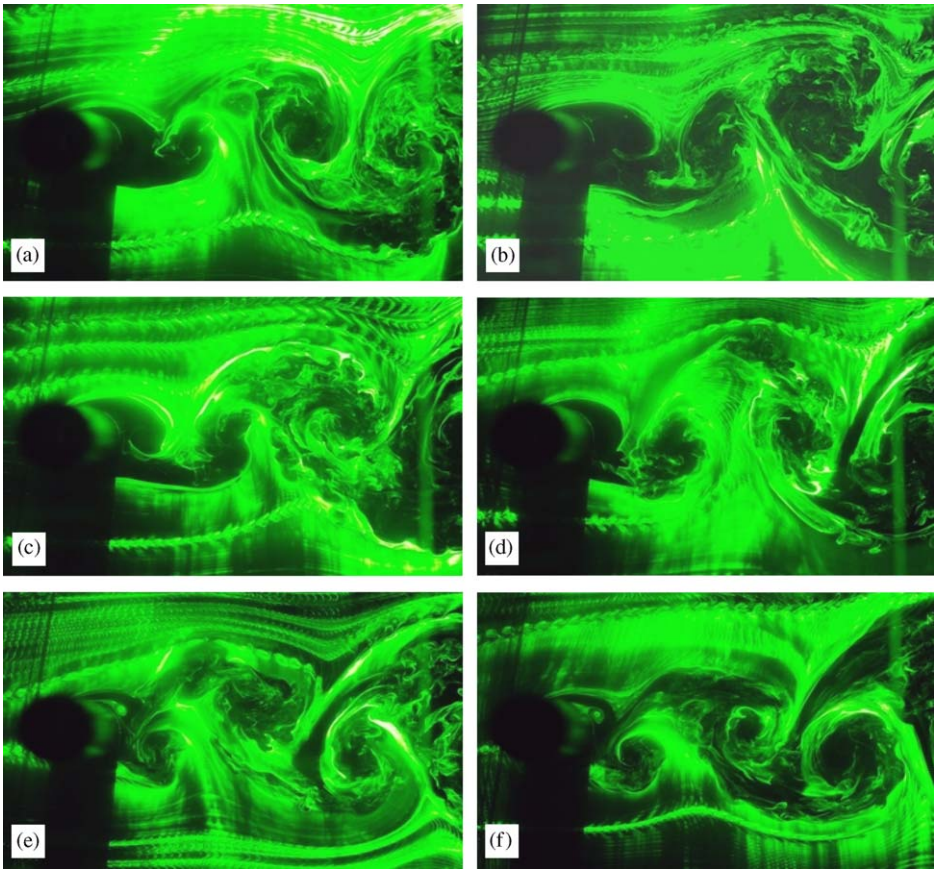

Fig. 15. Visualized flows in the vertical center plane according to the oscillation amplitude θ_A at $F_R = 1.0$. (a) $\theta_A = 10^\circ$, (b) $\theta_A = 20^\circ$, (c) $\theta_A = 30^\circ$, (d) $\theta_A = 40^\circ$, (e) $\theta_A = 50^\circ$, (f) $\theta_A = 60^\circ$.

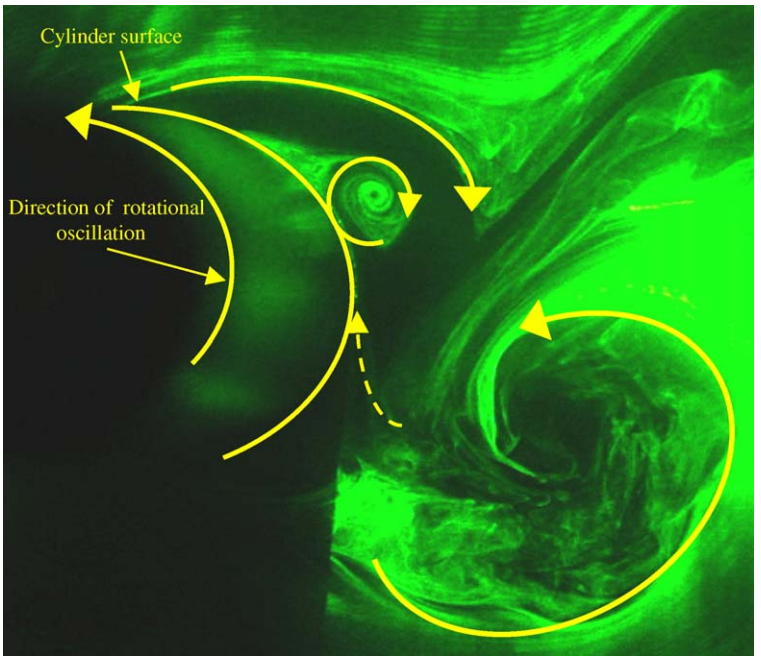

Fig. 16. Generation of a small-scale vortex in the shear layer just near the cylinder surface at $\theta_A = 60^\circ$ and $F_R = 1.0$.

4. Conclusions

The flow characteristics of the wake behind a rotationally oscillating circular cylinder were investigated experimentally with varying forcing conditions. The cylinder wake was found to show five flow regimes according to the forcing conditions, with each regime having distinct vortex shedding characteristics and wake structure. Forcing the cylinder to undergo rotational oscillatory motion was found to be effective for controlling the wake flow. This rotational oscillating motion increased the vorticity of the shear layer behind the cylinder and greatly affected the instability of the shear layer. The flow structure in the near wake was strongly dependent on the forcing condition. The length of the vortex formation region decreased as the frequency ratio F_R or the oscillation amplitude θ_A was increased. In addition, rotational oscillation of the cylinder at high F_R enhanced the flow separation and vortex coalescence.

When the lock-on phenomenon occurred at forcing frequencies near the natural vortex shedding frequency, the vortex shedding was in phase with the oscillatory motion of the cylinder. This phenomenon always occurs at the frequency ratio $F_R = 1.0$, and the frequency range centered on $F_R = 1.0$ expanded with increasing oscillation amplitude. In the lock-on flow regime, when the oscillation amplitude was less than the threshold amplitude $\theta_t = 8^\circ$, the lock-on phenomenon occurred only at the frequency ratio of $F_R = 1.0$. Moreover, the forced small-scale vortex was clearly observed when the oscillation amplitude is $\theta_A \geqslant 50^\circ$ at $F_R = 1.0$.

The maximum drag reduction was 32.82% in the low-frequency transition regime at $F_R = 0.8$ and 43.7% in the lock-on regime at $\theta_A = 60^\circ$, respectively. Thus, provided the forcing parameters are chosen appropriately, the rotational oscillation of a cylinder can be a promising method for controlling the drag acting on the cylinder. Importantly for practical applications, this approach is effective even at large Reynolds numbers.

Acknowledgment

This research was supported by National Research Laboratory (NRL) program of Ministry of Science and Technology (MOST), Korea.

References

Baek, S.J., Sung, H.J., 1998. Numerical simulation of the flow behind a rotary oscillating circular cylinder. Physics of Fluids 10, 869–876.

Bloor, M.S., 1963. The transition to turbulence in the wake of a circular cylinder. Journal of Fluid Mechanics 19, 290–304.
Choi, S.H., Choi, H.C., Kang, S.M., 2002. Characteristics of flow over a rotationally oscillating cylinder at low Reynolds number. Physics of Fluids 14, 2767–2777.
David, J., Gharib, M., 2004. On the relationship between the vortex formation process and cylinder wake vortex patterns. Journal of Fluid Mechanics 519, 161–181.
Dimotakis, P.E., 1978. Laser-Doppler velocimetry momentum defect measurement of cable drag at low to moderate Reynolds numbers. NCBC Report, Contract N62583/77-M-R541.
Filler, J.R., Marston, P.L., Mih, W.C., 1991. Response of the shear layers separating from a circular cylinder to small-amplitude rotational oscillations. Journal of Fluid Mechanics 231, 481–499.
Gerrard, J.H., 1954. A disturbance-sensitive Reynolds number range of the flow past a circular cylinder. Journal of Fluid Mechanics 22, 187–196.
Gerrard, J.H., 1966. The mechanics of the formation region of vortices behind bluff bodies. Journal of Fluid Mechanics 25, 401–413.
Graham, J.M.R., 1969. The effect of end-plates on the two-dimensionality of a vortex wake. The Aeronautical Quarterly 20, 237–247.
Koopman, G.H., 1967. The vortex wakes of vibrating cylinders at low Reynolds numbers. Journal of Fluid Mechanics 28, 501–512.
Mahfouz, F.M., Badr, H.M., 2000. Flow structure in the wake of a rotationally oscillating cylinder. ASME Journal of Fluids Engineering 122, 290–301.
Maskell, E.C., 1963. A theory of the blockage effects on bluff bodies and stalled wings in a closed wind tunnel. Report and Memoranda No. 3400, Aeronautical Research Council.
Ongoren, A., Rockwell, D., 1988. Flow structure from an oscillating cylinder: Part 1. mechanisms of phase shift and recovery in the near wake. Journal of Fluid Mechanics 191, 197–223.
Panton, R.L., 1996. Incompressible Flow, second ed. Wiley-Interscience, New York.
Shiels, D., Leonard, A., 2001. Investigation of a drag reduction on a circular cylinder in rotary oscillation. Journal of Fluid Mechanics 431, 297–322.
Stansby, P.K., 1974. The effects of end plates on the base pressure coefficient of a circular cylinder. Aeronautical Journal 78, 36–37.
Taneda, S., 1978. Visual observations of the flow past a circular cylinder performing a rotary oscillation. Journal of the Physical Society of Japan 45, 1038–1043.
Tokumaru, P.T., Dimotakis, P.E., 1991. Rotary oscillation control of a cylinder wake. Journal of Fluid Mechanics 224, 77–90.
Williamson, C.H.K., 1996. Vortex dynamics in the cylinder wake. Annual Review of Fluid Mechanics 28, 477–539.